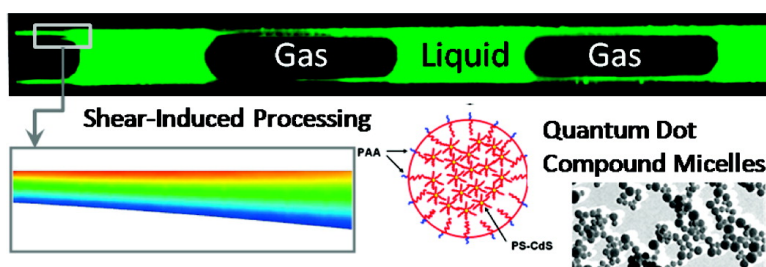# Langmuir

Letter

Formation and Shear-Induced Processing of Quantum Dot Colloidal Assemblies in a Multiphase Microfluidic Chip

Greg Schabas, Chih-Wei Wang, Ali Oskooei, Huda Yusuf, Matthew G. Moffitt, and David Sinton

More About This Article

Additional resources and features associated with this article are available within the HTML version:

- Supporting Information
- Access to high resolution figures
- Links to articles and content related to this article
- Copyright permission to reproduce figures and/or text from this article

View the Full Text HTML

Formation and Shear-Induced Processing of Quantum Dot Colloidal Assemblies in a Multiphase Microfluidic Chip

Greg Schabas,[†] Chih-Wei Wang,[‡] Ali Oskooei,[†] Huda Yusuf,[‡] Matthew G. Moffitt,*,[‡] and David Sinton*,[†]

Department of Mechanical Engineering, University of Victoria, P.O. Box 3055, Stn. CSC, Victoria, BC, Canada V8W 3P6, and Department of Chemistry, University of Victoria, P.O. Box 3065, Victoria, BC, Canada V8W 3V6

The controlled self-assembly of polymer-stabilized quantum dots (QDs) into mesoscale aqueous spherical assemblies termed quantum dot compound micelles (QDCMs) using a two-phase gas-segmented microfluidic reactor is described. Self-assembly is initiated by the fast mixing of water (~1 s) with a blend solution of polystyrene-coated QDs and amphiphilic polystyrene-*block*-poly(acrylic acid) stabilizing chains via chaotic advection within liquid plugs moving through a sinusoidal channel. Subsequent recirculating flow within a post-formation channel subjects the dynamic QDCMs to shear-induced processing, controlled via the flow rate and channel length, before a final quench into pure water. During processing, larger QDCMs within the initial population undergo breakup into smaller particles, resulting in smaller mean particle sizes, smaller relative standard deviations, and more skewed distribution shapes, as the overall shear exposure is increased. For these cases, shear-induced size reduction is sufficient to dominate surface tension-driven growth.

Introduction

The size-tunable optical and electronic properties of semiconductor and metal nanoparticles make them promising functional elements for a wide range of new materials and devices. However, future applications in photonics, sensing, and biological labeling will require the controlled self-assembly of nanoparticles into complex colloidal structures with hierarchical organization.[1–10] The spatial confinement and associated mass transport phenomena in microfluidic channels has been shown to be well suited to the controlled synthesis of inorganic[11–15] and polymeric[16,17] nanoparticles, and also to the self-assembly of various nanostructures from molecular building blocks, including microcapsules,[18] vesicles,[19] and bilayer membranes.[20] Microfluidic environments also offer immense potential for the controlled self-assembly of nanoparticles into higher-order structures,[21,22] since associated self-assembly events are strongly dependent on a number of factors, including local concentrations of reagents (e.g., nanoparticle concentrations, pH, water content), mixing rates, and shear forces, which can be finely tuned in a microfluidic device. Another demonstrated advantage of microfluidics for nanoparticle formation and self-assembly is the potential separation of formation and growth processes for improved size distribution control, as shown recently by the synthesis of inorganic nanocrystals in a two-temperature microreactor.[12]

Our research has demonstrated the self-organization of block copolymer-stabilized quantum dots (QDs) into mesoscale spherical assemblies termed quantum dot compound micelles (QDCMs) (Figure 1a).[22–24] The resulting assemblies possess complex structural hierarchy, water solubility, and versatile surface chemistry, which make them promising colloidal elements for biological labeling, sensing, and photonics. Blends of block copolymer-stabilized cadmium sulfide (CdS) QDs with external polystyrene (PS) brush layers (PS-CdS) and polystyrene-*block*-poly(acrylic acid) (PS-*b*-PAA) stabilizing chains codissolved in polar organic solvents (e.g., dimethylformamide, DMF) spontaneously form QDCMs above a critical water concentration (cwc ~2 wt % for a 2 wt % polymer solution).[24] The process is driven by phase separation of PS blocks of PS-CdS and PS-

* To whom correspondence should be addressed. E-mail: mmoffitt@uvic.ca (M.G.M.); dsinton@me.uvic.ca (D.S.). Telephone: (250) 721-7162 (M.G.M.); (250) 721-8623(D.S.). Fax: (250) 721-7147 (M.G.M.); (250) 721-6051 (D.S.).

† Department of Mechanical Engineering.

‡ Department of Chemistry.

(1) Alivisatos, A. P. *Science* **1996**, *271*, 933.

(2) Murray, C. B.; Kagan, C. R.; Bawendi, M. G. *Annu. Rev. Mater. Sci.* **2000**, *30*, 545.

(3) Boal, A. K.; Ilhan, F.; DeRouchey, J. E.; Thurn-Albrecht, T.; Russel, T. P.; Rotello, V. M. *Nature* **2000**, *404*, 746.

(4) Pileni, M. P. *J. Phys. Chem. B* **2001**, *105*, 3358.

(5) Caruso, F. *Adv. Mater.* **2001**, *13*, 11.

(6) Faul, C. F. J.; Antonietti, M. *Adv. Mater.* **2003**, *15*, 673.

(7) Lin, Y.; Skaff, H.; Emrick, T.; Dinsmore, A. D.; Russell, T. P. *Science* **2003**, *299*, 226.

(8) Tang, Z.; Kotov, N. A. *Adv. Mater.* **2005**, *17*, 951.

(9) Shenhar, R.; Norsten, T. B.; Rotello, V. M. *Adv. Mater.* **2005**, *17*, 657.

(10) Kim, B.-S.; Qiu, J.-M.; Wang, J.-P.; Taton, T. A. *Nano Lett.* **2005**, *5*, 1987.

(11) Krishnadasan, S.; Tovilla, J.; Vilar, R.; deMello, A. J.; deMello, J. C. *J. Mater. Chem.* **2004**, *14*, 2655.

(12) Yang, H.; Luan, W.; Tu, S.; Wang, Z. M. *Lab Chip* **2008**, *8*, 451.

(13) (a) Chan, E. M.; Mathies, R. A.; Alivisatos, A. P. *Nano Lett.* **2003**, *3*, 199. (b) Chan, E. M.; Alivisatos, A. P.; Mathies, R. A. *J. Am. Chem. Soc.* **2005**, *127*, 13854.

(14) Yen, B. K. H.; Gunther, A.; Schmidt, M. A.; Jensen, K. F.; Bawendi, M. G. *Angew. Chem., Int. Ed.* **2005**, *44*, 5447.

(15) Cottam, B. F.; Krishnadasan, S.; DeMello, A. J.; DeMello, J. C.; Shaffer, M. S. P. *Lab Chip* **2007**, *7*, 167.

(16) (a) Nie, Z.; Li, W.; Seo, M.; Xu, S.; Kumacheva, E. *J. Am. Chem. Soc.* **2006**, *128*, 9408. (b) Seo, M.; Nie, Z.; Xu, S.; Mok, M.; Lewis, P. C.; Graham, R.; Kumacheva, E. *Langmuir* **2005**, *21*, 11614.

(17) Karnik, R.; Gu, F.; Basto, P.; Cannizzaro, C.; Dean, L.; Kyei-Manu, W.; Langer, R.; Farokhzad, O. C. *Nano Lett.*, published online July 26, http://dx.doi.org/10.1021/nl801736q.

(18) Steinbacher, J. L.; Moy, R. W. Y.; Price, K. E.; Cummings, M. A.; Roychowdhury, C.; Buffy, J. J.; Olbricht, W. L.; Haaf, M.; McQuade, D. T. *J. Am. Chem. Soc.* **2006**, *128*, 9442.

(19) Jahn, A.; Vreeland, W. N.; Gaitan, M.; Locascio, L. E. *J. Am. Chem. Soc.* **2004**, *126*, 2674.

(20) Malmstadt, N.; Nash, M. A.; Purnell, R. F.; Schmidt, J. J. *Nano Lett.* **2006**, *6*, 1961.

(21) Chang, J.-Y.; Yang, C.-H.; Huang, K.-S. *Nanotechnology* **2007**, *18*, 1.

(22) Schabas, G.; Yusuf, H.; Moffitt, G.; Sinton, D. *Langmuir* **2008**, *24*, 637.

(23) Moffitt, M.; Vali, H.; Eisenberg, A. *Chem. Mater.* **1998**, *10*, 1021.

(24) Yusuf, H.; Kim, W.-G.; Lee, D.-H.; Guo, Y.; Moffitt, M. G. *Langmuir* **2007**, *23*, 868.
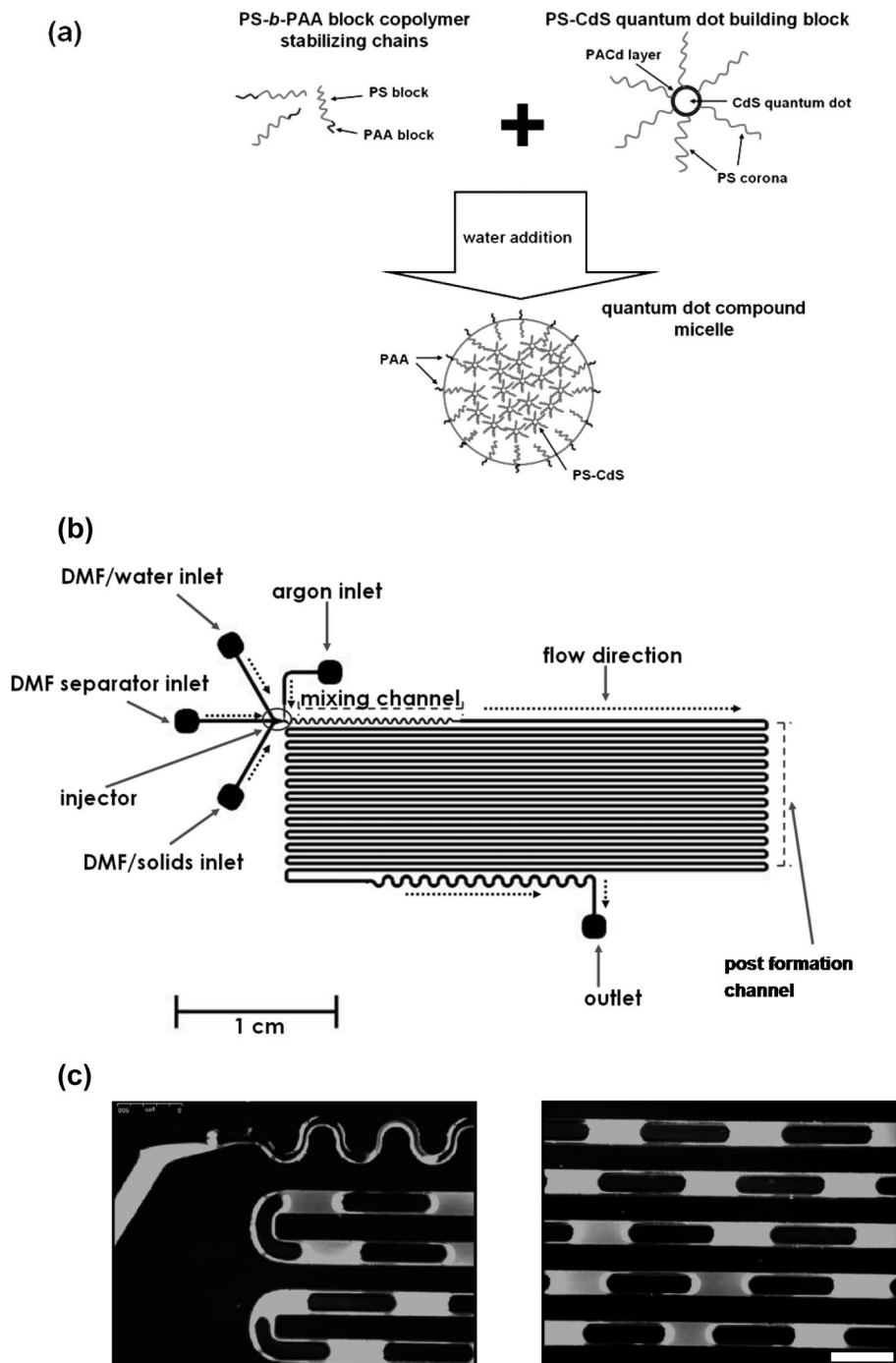
(a)

PS-*b*-PAA block copolymer stabilizing chains

PS-CdS quantum dot building block

PS block
PAA block

PACd layer
CdS quantum dot
PS corona

water addition

quantum dot compound micelle

PAA
PS-CdS

(b)

DMF/water inlet
argon inlet
DMF separator inlet
mixing channel
flow direction
injector
DMF/solids inlet
post formation channel
outlet
1 cm

(c)

Figure 1. QDCM assembly process and multiphase microfluidic reactor approach. (a) Schematic of the QDCM assembly process. Gray indicates hydrophobic blocks, while black indicates hydrophilic blocks. (b) Schematic of the microfluidic reactor. The solid constituent and water-containing streams are combined with a separating solvent stream prior to injection of the argon gas bubbles, which compartmentalize the liquid and facilitate rapid mixing and shearing of reactants and products. (c) Select fluorescence microscopy images of the reactor in operation. The white scale bar indicates 500 μm.

b-PAA from solution, with the PAA blocks of the stabilizing chains maintaining colloidal stability in water. Interfacial tension drives QDCM particle growth at water concentrations above the cwc. On the other hand, increasing water concentration decreases the QDCM growth dynamics: as more water is added, DMF solvent is leached from the polymer phase, resulting in decreased mobility of the PS chains, with the particles ultimately becoming frozen on experimental time scales above a water concentration of ~8−11 wt %.[25] Therefore, by controlling the rates of water addition and mixing relative to the dynamics of particle growth,

QDCM sizes can be tuned. However, improved methods offering finer control over the sizes and polydispersities of colloidal QD assemblies are clearly of interest for various future applications.[22,24,26]

In previous work, QDCMs were formed through steady dropwise water addition to a stirred bulk solution, with kinetic control of particle sizes demonstrated via the initial polymer concentration or the speed of water addition.[24] More recently, we employed a single-phase flow-focusing microfluidic reactor

(25) Zhang, L.; Shen, H.; Eisenberg, A. *Macromolecules* **1997**, *30*, 1001.

(26) Yusuf, H.; Kim, W.-G.; Lee, D.-H.; Aloshyna, M.; Brolo, A. G.; Moffitt, M. G. *Langmuir* **2007**, *23*, 5251.

strategy, in which QDCM formation was initiated in a central stream via cross-stream diffusion of water from a surrounding sheath stream followed by a downstream quench step;[22] on-chip size control was exerted via either the steady-state water concentration or the flow rate. However, QDCM polydispersies via this microfluidic approach were comparable to those obtained via the bulk method (~30% relative standard deviations), which may be partially attributed to the limitations of diffusion-controlled mixing and large residence time distributions characteristic of single-phase reactors. In contrast, multiphase microfluidic reactor strategies offer the potential advantages of improved mixing and narrower residence time distributions.

In multiphase microfluidic reactors, interfaces between immiscible phases serve to compartmentalize reactants into droplets or plugs,[27,28] effectively narrowing the residence time distribution in both phases compared to single-phase systems. The residence time distribution is narrowed significantly for the continuous (wetting) phase and becomes effectively discrete for the discontinuous (droplet) phase. An important byproduct of phase-wise segregation of reactants is the development of internal flow structures within the droplets or plugs, which can dramatically increase reagent mixing, particularly in sinusoidal microfluidic channels that serve to break the symmetry of the flow pattern.[27] In one common multiphase system, an oil with a large tendency to wet the microfluidic channel walls forms the continuous phase, containing droplets of the aqueous solutions of interest.[27,28] To facilitate gas−liquid reactions, and reactions in nonaqueous solutions, gas−liquid segmented reactors have also been developed,[14] in which the droplet phase consists of discrete bubbles of a gas within a liquid continuous phase. In the context of particle systems, the advantages of multiphase microfluidic reactors have found application in the synthesis of CdSe QDs,[14] the synthesis of colloidal silica particles,[29] and protein crystallization.[30]

In this work, we apply a gas−liquid multiphase microfluidic reactor to induce QDCM formation via water addition and self-assembly. The self-assembling components in DMF are combined with a concentration of water above the cwc (but below the range where QDCMs become kinetically frozen); the stream is segmented by gas bubbles in a sinusoidal mixing channel, such that chaotic advection within the liquid phase results in rapid mixing and QDCM formation. The sinusoidal mixing channel is followed by a post-formation channel of variable length (L), in which the formed QDCMs are subject to recirculating flow within the fluid segments for variable times and at variable shear rates, prior to an off-chip quench step and size distribution analysis. The post-formation channel was intended to provide time for QDCM growth in the discrete liquid plugs, with narrow residence time distributions as a result of compartmentalization. However, we find that recirculating flow within the liquid segments results in shear-induced breakup of QDCMs into smaller assemblies, decreasing mean particle sizes and narrowing size distributions. This influence is sufficient to counteract interfacial tension-driven growth. These surprising results point to new opportunities for using controlled shear forces in microfluidic environments for self-assembly, not only to effect fast mixing of components but also to tune size distributions of assemblies via post-formation processing.

(27) Song, H.; Tice, J. D.; Ismagilov, R. F. *Angew. Chem.* **2003**, *42*, 768.
(28) Gunther, A.; Jensen, K. F. *Lab Chip* **2006**, *6*, 1487.
(29) Khan, S. A.; Gunther, A.; Schmidt, M. A.; Jensen, K. F. *Langmuir* **2004**, *20*, 8604.
(30) Zheng, B.; Tice, J. D.; Ismagilov, R. F. *Adv. Mater.* **2004**, *16*, 1365.

Experimental Section

Materials. All block copolymer samples were synthesized via anionic polymerization of the associated polystyrene-*block*-poly(*tert*-butyl acrylate) block copolymer, followed by hydrolysis of the ester block; numbers in brackets refer to number-average degrees of polymerization of each block.[24] Block copolymer-stabilized CdS QDs with an external PS brush layer (PS-CdS) were synthesized via self-assembly of a PS(300)-*b*-PAA(12) block copolymer to form reverse micelles in a hydrophobic solvent, followed by templated CdS QD synthesis in the micelle cores, as described in ref 24. Static and dynamic light scattering carried out in DMF solvent revealed that each stable PS-CdS particle is surrounded by an average of 54 ± 2 copolymer chains (kinetically frozen at the QD surface by the high T_g of the poly(cadmium acrylate), PACd, surface layer) and has a z-average hydrodynamic diameter of $d_h = 36 \pm 2$ nm. QDCMs were formed via the addition of water to solutions of PS-CdS and PS(665)-*b*-PAA(68) stabilizing chains codissolved in DMF.

For microfluidic self-assembly experiments, PS-CdS and PS(665)-*b*-PAA(68) stabilizing chains were dispersed separately in DMF (99.9+% HPLC grade, H_2O < 0.03%), each at a total solids concentration of 2 wt %; the solution of stabilizing chains and dispersion of PS-CdS were then combined to form a 50/50 (w/w) blend of constituents in DMF. This solution was then further diluted with additional DMF to yield a solution with 1 wt % solids in DMF. A DMF/water mixture was created by adding 99.9% pure deionized water to DMF on a digital balance (Denver Instruments) to produce a mixture containing 12 wt % water, which yielded a steady-state water content of 4% when combined with the two other liquid streams at equal flow rate. Fluorescein powder (Invitrogen) was dissolved in water at a concentration of 0.2 mM; the fluorescein/water solution was then mixed with DMF to produce a DMF/fluorescein/water solution containing approximately 50 wt % water.

Microchannel Fabrication. Negative masters were fabricated on glass slides using a negative photoresist, SU-8 (Microchem Inc., MA). Prior to use, the glass slides were cleaned and heated on a hotplate to remove all moisture. A 50 μm thick film of photoresist was spin-coated on top of a glass slide. The glass slide was then heated to 95 °C to evaporate the solvents from the photoresist. A photomask was placed over the film and the device was exposed to UV light for 90 s. After additional heating, the device was submerged in SU-8 developer (Microchem Inc., MA) to remove unexposed photoresist.

The microfluidic chip was fabricated from poly(dimethylsiloxane), PDMS, using a SYLGARD 184 silicone elastomer kit with an elastomer base to curing agent ratio of 10:1. The elastomer and curing agent were mixed together and poured onto the photoresist masters in a Petri dish. The Petri dish was placed in a vacuum chamber to remove air bubbles from the PDMS, followed by PDMS curing at $T = 85$ °C. The microfluidic reactor was peeled off the master, and holes were punched through its reservoirs to allow for the insertion of tubing. A thin PDMS film was produced on top of a glass slide by spin-coating and was permanently bonded to the base of the microfluidic reactor after both components were exposed to oxygen plasma.

Flow Delivery and Imaging. Pressure-driven flow to the inlets of the reactors was provided using 50, 100, and 250 μL gastight syringes (Hamilton, NV) mounted on syringe pumps (Harvard Apparatus, MA). Flow rates were controlled via the syringe pumps. The syringes connected to the microfluidic chip via 1/16th inch (OD) Teflon tubing.

Fluorescence images of the reactor were captured using a CCD camera (AF6000 Orca, Hamamatsu) installed on an inverted microscope (DMI 6000B, Leica). The filter cube employed to image the QD emission transmitted light in the range 350−400 nm to the chip, and returning light above 500 nm to the camera. The fluorescein filter cube transmitted light in the range 450−500 nm chip, and returning light in the range 510−560 nm to the camera. While the emission spectra of the fluorescein and QDs overlapped, their contributions could be separated via distinct excitation bands; that is, the QDs showed negligible response to the excitation light

employed for fluorescein imaging and vice versa. Image normalization was employed to facilitate comparison of light emissions from QDCMs as compared to the base case of QD fluorescence and to remove nonuniformities in illumination and the image field. An image of the chip filled with the fluorescent DMF/solids phase provided the bright field, and similarly, an image of the chip filled with DMF provided the dark field. Fluorescein images were also similarly normalized such that fluorescent intensity could be related to species concentration. In those cases, the DMF/fluorescein/water phase constituted the bright field and the DMF/solids phase constituted the dark field.

Transmission electron microscopy (TEM) of various aqueous QDCM colloids was performed (Hitachi H-700 electron microscope) operating at an accelerating voltage of 75 kV. For off-chip QDCM size distribution analysis, QDCM dispersions were collected from the chip following the post-formation channel into vials containing a large excess of deionized water, where the particles immediately become kinetically frozen due to the high water content. The estimated solids content of the final aqueous dispersions was 0.25 mg/mL. A $\sim$10 μL drop of each QDCM dispersion was deposited on a carbon-coated Formvar 300 mesh copper grid and then shadowed with Pt/Pd wire for imaging. Particle size analysis and statistics were carried out on the shadowed samples, with various regions of the TEM grid randomly sampled and 300 particles measured and included in each analysis. Images of selected samples were also taken without Pt/Pd shadowing, in order to characterize the QDCM internal structure.

Dynamic Light Scattering (DLS). All DLS experiments were carried out on a Brookhaven Instruments photon correlation spectrometer equipped with a BI-200SM goniometer, a BI-900AT digital autocorrelator, and a Melles Griot He−Ne laser (632.8 nm) with maximum power output of 75 mW. All DLS measurements were conducted at 23 °C. Off-chip DLS analysis of QDCM samples collected from the microfluidic reactor were conducted in deionized water at a single scattering angle of 90°. For each sample, DLS was carried out for four different solution concentrations between 0.1 and 0.01 mg/mL. For each solution concentration, three repeat measurements of the autocorrelation function were obtained. Single-particle hydrodynamic radii (r_h) were determined by extrapolation of effective hydrodynamic radii at different concentrations (determined from cumulant analysis) to infinite dilution.

Results and Discussion

The QDCM assembly process and the gas−liquid segmented microfluidic reactor strategy are shown in Figure 1. The stream containing the PS-CdS and PS-*b*-PAA constituents in DMF is combined with a separating DMF and a DMF−water stream prior to injection of the argon gas. The gas bubbles compartmentalize the colaminar liquid flow of reactants into liquid plugs, which facilitate rapid mixing of reactants in the sinusoidal channel similar to previous microfluidic reactors.[27,28] The chip was fabricated using established soft-lithography methods and a set channel depth of 150 μm. The mixing channel was 100 μm wide and 100 mm in length, and the post-formation channel was 200 μm wide and either $L = 200$ mm or $L = 740$ mm depending on the chip. Quenching (kinetic freezing) of the particles was achieved off-chip by connecting the outlet directly to a vial containing $\sim$250 μL of water via 7 cm, $d = 250$ μm tubing. Visualization of the mixing processes was performed with an inverted fluorescence microscopy system with excitation/emission filter combinations for QD fluorescence ($\lambda_{ex} = 350-400$ nm, $\lambda_{em} > 500$ nm) and fluorescein ($\lambda_{ex} = 450-500$ nm, $\lambda_{em} = 510-560$ nm). Particle size distribution analysis was performed off-chip using transmission electron microscopy. Select fluorescence microscopy images of the reactor in operation are given in Figure 1c, where the observed fluorescence is that of the QDs in individual PS-CdS or QDCM assemblies. In all cases presented here, the initial polymer solution was composed of a 50/50

(w/w) mixture of PS-CdS and PS(665)-*b*-PAA(68) stabilizing chains (where numbers in brackets indicate number-average degrees of polymerization of the blocks), dissolved to a 1 wt % total solid content in DMF. For the case shown in Figure 1c, and for most preparations in this paper, the steady-state water content was held constant at 4 wt %, such that it was above the cwc ($\sim$2%)[24] but below the range of water content where QDCMs become kinetically frozen on experimental time scales ($\sim$8−11%).[25] The mixing visualization experiments were an exception, in which the steady-state water content was 33 wt % as required for effective tracking of the water via fluorescein dye. The liquids and Ar gas were delivered to the chip via syringe pumps, with nominal total flow rates of either $Q = 4.8$ or 24 μL/min. In both cases, the nominal ratio of total liquid to gas flow was 1:3, and the flow rates at each of the three liquid inlets were equal, at 0.4 and 2.0 μL/min for the $Q = 4.8$ μL/min and $Q = 24$ μL/min cases, respectively.[31]

In order to characterize the mixing process in the sinusoidal channel, a small amount of fluorescein was added to the water component for a trial in which the steady-state water concentration was 33 wt % and the flow rate was $Q = 4.8$ μL/min, corresponding to an average channel velocity of 2.7 mm/s. Figure 2a shows the fluorescein emission, which tracks the water distribution, and Figure 2b shows the QD emission, each at 0, 2, and 5 mm downstream locations from the injector. From Figure 2a, the fluorescein had evenly spread throughout the liquid plug once the segment had traveled 2 mm downstream from the injector. This suggests that the water was fully mixed within the liquid plugs in less than 1 s after the reactants were combined at the injector; the mixing is expected to be even faster at higher flow rates, due to increased shear within the liquid plugs. In contrast, it took approximately 12 s to achieve full mixing of water to the same steady-state water concentration (33 wt %) in the diffusion-controlled flow-focusing reactor.[22] In Figure 2b, the increased brightness in the QD signal during mixing provides a direct visualization of local QDCM formation, due to increased light scattering from larger particles following self-assembly.[22] In this series of images, fluorescence streamlines of increased brightness are visible, providing an indication of the advection patterns and subsequent mixing inside the liquid plug. While the water is mixed in the first second after the injector, the QDCM particles, which form as a result of water mixing, are completely dispersed within the liquid plug by the 5 mm downstream location, only 2 s after leaving the injector. These results therefore point to greatly enhanced mixing in the gas-segmented reactor compared to our previous flow-focusing strategy.

Off-chip analysis of QDCM populations obtained for three different conditions of post-formation channel length (L) and flow rate (Q) at a constant steady-state water concentration of 4 wt % was carried out by TEM. A representative TEM image of QDCMs formed in the $L = 740$ mm reactor at a total flow rate of $Q = 4.8$ μL/min is shown in Figure 3a. Figure 3b shows a higher magnification image of the same QDCM population without Pt/Pd shadowing prior to imaging, allowing the internal structure of the assemblies to be visualized. Consistent with the schematic of the QDCM structure in Figure 1a, well-dispersed CdS QDs (dark dots) can be clearly seen distributed within the dark gray spheres of self-assembled PS chains. The aggregation of QDCM particles observed in the TEM images is an artifact of solvent evaporation on the TEM grid; dynamic light scattering

(31) Due to leakage and compressibility effects, as experienced by others with similar systems, it is likely that the actual total argon flow rates are less than those indicated by the pumps and nominally gastight syringes. In this work, the liquid reactant flow rates are specified, with the total flow rates containing the gas component considered nominal.
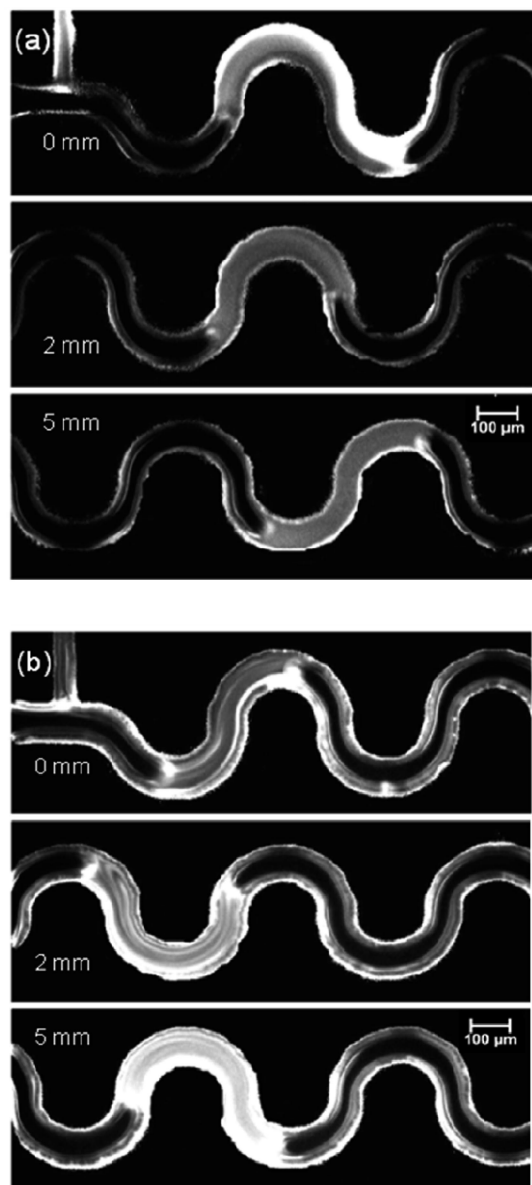
Figure 2. Reactant mixing and QDCM formation in the gas–liquid segmented reactor. (a) Normalized fluorescein emission taken at three downstream locations in the mixing channel. Fluorescein was employed as a water tracer, and the steady-state water concentration was 33 wt %. The images were captured at the various downstream distances indicated. Mixing of the tracer indicates that water was effectively mixed throughout the plug by the 2 mm downstream location (<1 s). (b) Corresponding images of QD emission in the mixing channel for the same case. The advection patterns within the plug are apparent as is the increased brightness attributed to increased light scattering due to the formation of QDCM particles.

(DLS) of the different particle populations suggests that the QDCMs are well-dispersed colloids in water.[32] Excellent colloidal stability was found for time periods of over 1 year. Particle size distributions, along with mean particle sizes and standard deviations, corresponding to TEM results for different QDCM self-assembly conditions are shown in Figure 4a–c. We now

<hr>

(32) Hydrodynamic radii, r_h, obtained from DLS for the various particle populations in deionized water (90° scattering angle, extrapolation to infinite dilution), were typically 20–30 nm larger than mean particle radii determined by TEM. This is consistent with the presence of a fully-stretched solvated PAA layer (~20 nm) surrounding the PS core of the QDCMs and indicates that particle agglomeration in solution is not significant. In addition, CONTIN size distribution analysis of DLS autocorrelation functions typically revealed monomodal size distributions, further suggesting the absence of colloidal agglomerates.
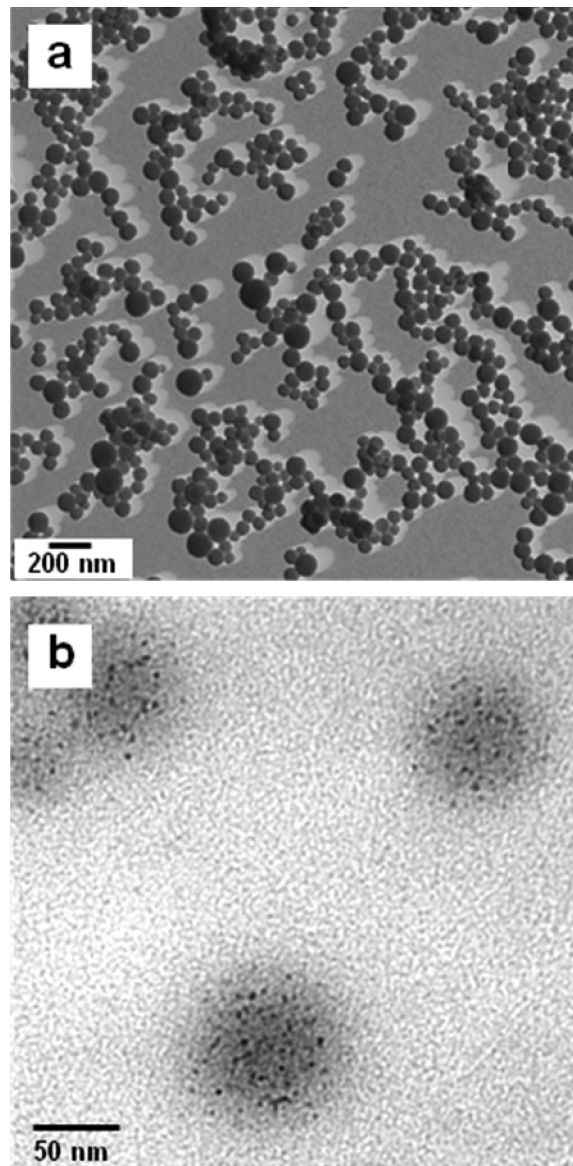

Figure 3. Representative TEM images of QDCMs prepared in a gas–liquid reactor with $L = 740$ mm at a steady state water concentration of 4 wt % and a flow rate of $Q = 4.8$ μL/min. In (a), the particles have been shadowed with Pt/Pd alloy prior to imaging; (b) shows QDCMs without shadowing, revealing the internal structure of multiple QDs.

turn to analysis of the effects of the channel length (L) and flow rate (Q) on the observed particle distributions.

For QDCMs prepared using the shorter post-formation channel ($L = 200$ mm) at the lower flow rate ($Q = 4.8$ μL/min), the resulting size distribution reveals a mean QDCM diameter of $d = 81$ nm with a relative standard deviation of $sd = 30\%$ (Figure 4a). This mean size and distribution width are very similar to those obtained for QDCM populations prepared at the same average water content (4.0 wt %) using our previous flow-focusing microfluidic device (e.g., $d = 81$ nm, sd = 27% for $Q = 9$ μL/min).[22] This suggests that the final water concentration is a predominant factor in determining the mean QDCM size following self-assembly. As well, we find comparable size heterogeneities (~30% relative standard deviations) arising from QDCM self-assembly via the two mixing strategies, despite the dramatic increase in the rate of mixing on the multiphase chip compared to diffusion-controlled mixing using the flow-focusing chip. This surprising result may be related to intrinsic size heterogeneities arising from the spinodal decomposition mech-
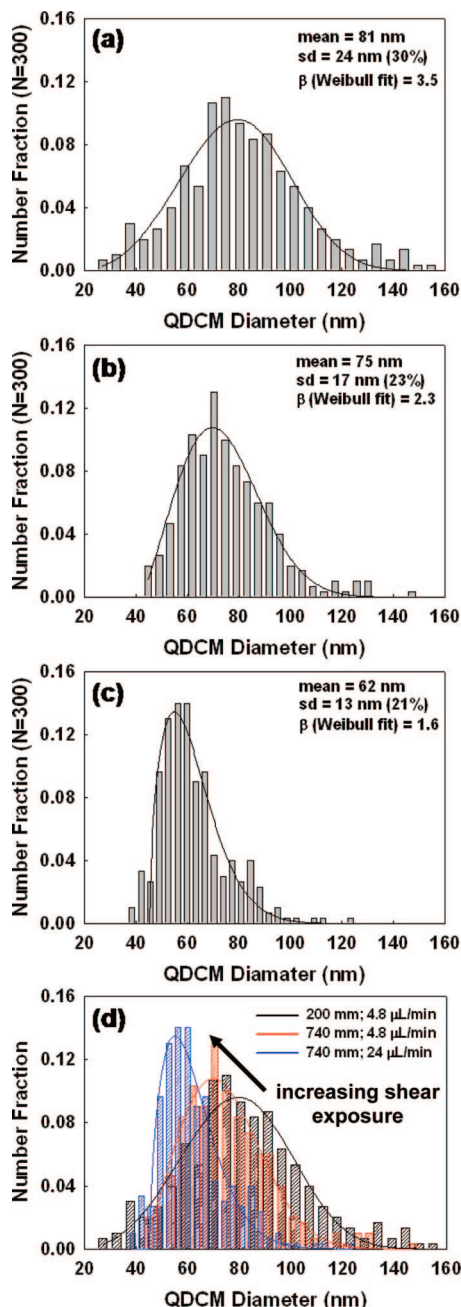
Figure 4. Particle size distributions, along with mean particle sizes and standard deviations, corresponding to TEM results for different QDCM self-assembly conditions. (a) Short post-formation channel ($L = 200$ mm) at the low flow rate ($Q = 4.8 \, \mu$L/min). (b) Long post-formation channel ($L = 740$ mm) at the low flow rate ($Q = 4.8 \, \mu$L/min). An increase in residence time (from 75 to 277 s) is found to effect a decrease in particle size. (c) Long post-formation channel ($L = 740$ mm) at the high flow rate ($Q = 24 \, \mu$L/min). Residence times in (a) and (c) are comparable, although in (c) the particles are exposed to significantly higher average shear rate, resulting in smaller particles with a lower polydispersity.

anism for QDCM formation above the cwc,[24] as well as to the very fast time scale of self-assembly and initial growth compared to the fastest demonstrated mixing time (∼1 s). Further investigations of the effect of water concentration on QDCM mean size and distribution widths within the two-phase reactor is the subject of ongoing experiments.

When the length of the post-formation channel following the mixing channel was increased to $L = 740$ mm at the same flow

rate ($Q = 4.8 \, \mu$L/min), the mean particle size decreased to $d = 75$ nm and the size distribution also became narrower, sd = 23% (Figure 4b). We note that the conditions for QDCM formation in the mixing channel are identical in the two experiments described in Figure 4a and b ($L = 200$ and 740 mm, $Q = 4.8 \, \mu$L/min), since both the water concentration and rate of mixing are the same for constant flow rate. However, the longer post-formation channel increases the residence time between QDCM formation and off-chip quenching from 75 to 277 s, based on a channel velocity of 2.65 mm/s corresponding to the flow rate $Q = 4.8 \, \mu$L/min. It was originally expected that interfacial tension-driven particle growth would result in increased QDCM size with increased time in the channel, although the above results indicate the opposite trend. This suggests a time-dependent counteracting influence of shear due to recirculating flow within the liquid segments as QDCMs pass through the post-formation channel.

To confirm this effect, we investigated QDCM formation on the $L = 740$ mm chip at an increased flow rate of $Q = 24 \, \mu$L/min. Under these conditions (Figure 4c), we found the smallest mean QDCM size of the three experiments, $d = 62$ nm, and the narrowest distribution width, sd = 21%. At this increased flow rate, the channel velocity is 13.3 mm/s, resulting in a residence time of 55 s in the 740 mm channel, comparable to the residence time of 75 s for the shorter-channel/lower-flow rate experiment described in Figure 4a ($L = 200$ mm, $Q = 4.8 \, \mu$L/min). However, in Figure 4c, the particles are exposed to significantly higher average shear rate due to the factor of 5 increase in the flow rate compared to Figure 4a, resulting in relatively smaller particles with a lower polydispersity.

Based on these trends, we conclude that QDCMs originally formed in the mixing channel experience shear-induced breakup as a result of recirculating flow within the post-formation channel, resulting in a decrease in mean particle size and polydispersity as the residence time or average shear rate is increased. We note that QDCM sizes and polydispersities decrease with increased residence times under the same shear conditions (Figure 4a and b), but also decrease with increased shear rate at roughly equivalent residence times (Figure 4a and c). Based on the resulting distributions, we conclude that post-formation shear effects increase for the three experiments in order from Figure 4a−c, such that short residence time/low shear is designated low shear exposure (Figure 4a), long residence time/low shear is designated intermediate shear exposure (Figure 4b), and short residence time/high shear is designated high shear exposure (Figure 4c). We note that long residence time/high shear conditions could also be achieved in principle, although such experiments would require a chip with a much longer post-formation channel than those investigated here.[33]

Along with the observed decrease in both the mean QDCM size and relative standard deviation with increasing shear exposure, we also note a concomitant change in the shape of the particle size distribution, which further supports shear-induced QDCM breakup following self-assembly. This change in the distribution shape was quantified using a Weibull probability density function:

$$f(d) = \frac{\beta}{\eta} \left(\frac{d - \gamma}{\eta} \right)^{\beta - 1} e^{-\left(\frac{d - \gamma}{\eta} \right)^{\beta}} \tag{1}$$

where d is the QDCM diameter and β, η, and γ are shape, scale, and location parameters of the Weibull function. Fits to this function are shown for each of the size distributions in Figure

---

(33) For example, to achieve a residence time of 277 s at a flow rate of $Q = 24 \, \mu$L/min, a post-formation channel of $L = $ ∼3700 mm would be required.

4. The shape parameter, β, characterizes the skew of a given distribution, with $\beta = 3.4$ indicating an approximately normal distribution and lower values of β describing more positive skew. The β values from Weibull fits to the QDCM size distributions for the three different experiments are indicated in Figure 4. In the case of low shear exposure (Figure 4a), a shape parameter of $\beta = 3.5$ was determined from the fit, confirming an approximately normal distribution of QDCM sizes arising from self-assembly with minimal post-formation processing. With intermediate shear exposure (Figure 4b), the shape parameter decreases to $\beta = 2.3$ and then decreases further to $\beta = 1.6$ for high shear exposure (Figure 4c). This indicates an increase in the positive skew of the distribution with increasing shear exposure. By overlapping the three distributions (Figure 4d), further insight into the development of the size distributions with post-formation processing is obtained. First, we notice that particles with $d < 40$ nm, which are observed at low shear exposure (black distribution), disappear at intermediate (red distribution) and high (blue distribution) shear exposure; this is attributed to some coalescence of extremely small particles via a combination of interfacial tension and shear effects. More importantly, comparison of the distributions shows a significant decrease in the fraction of particles with sizes greater than ~70 nm and a concomitant increase in the fraction of smaller particles with sizes centered ~50 nm as the shear exposure is increased. The progressive shift to smaller sizes, along with a narrowing and positive skewing of the distributions, is therefore attributed to preferential breakup of particles larger than ~70 nm upon post-formation shear exposure.

To evaluate the feasibility of shear-induced droplet breakup following QDCM self-assembly, we consider the capillary number, Ca, which describes the balance of viscous to interfacial forces for dispersed liquid drops under shear:

$$Ca = \frac{\eta_m \dot{\gamma} D}{2\Gamma} \tag{2}$$

where η_m is the viscosity of the matrix, $\dot{\gamma}$ is the shear rate, D is the diameter of the undeformed drop, and Γ is the dispersed phase/matrix phase interfacial tension.[34,35] For steady shear rates above the critical capillary number, Ca_c, drops will undergo breakup into smaller drops. A key feature of eq 2 is that larger drops are more susceptible to shear-induced breakup than smaller drops, which is consistent with the observed skewing of the QDCM distribution shape with increased shear exposure in the microchannel.

The critical value Ca_c is a strong function of the viscosity ratio of the dispersed phase over that of the matrix phase, λ, and also depends on the type of flow field and the flow history.[34–36] In the present case of DMF-swollen QDCM particles dispersed in a DMF/water matrix, the viscosity ratio is extremely high, $\lambda \gg 10$. For high viscosity drops under purely extensional flow fields, or in flow fields of relatively low vorticity, experimental results predict Ca_c values of ~0.1 in the case of steady flow.[34–36] For the viscosity of the matrix phase, we assume $\eta_m = 0.92 \times 10^{-2}$ P, which is the value for pure DMF, considering that the steady-state water content is relatively low (4 wt %). Therefore, using an interfacial tension value of $\Gamma = 2$ dyn/cm, determined via a simplified treatment of QDCMs as DMF-swollen polystyrene particles dispersed in DMF/water (see the Supporting Information) and $D = 100$ nm, substitution of $Ca_c = 0.1$ into eq 2 predicts

a shear rate of 4×10^6 s^{-1} to effect QDCM breakup. In the high-viscosity particle case, this critical shear rate will increase sharply toward infinity as the flow vorticity increases to the limit of simple shear flow.[34–36]

Although the above treatment provides a point of reference, it is important to note that several additional features of our system make this simplified calculation unrealistic, and account for QDCM breakup at the considerably lower shear rates present within the gas-segmented reactor. For instance, the above calculation assumes steady shear conditions, whereas strong shear gradients are an important feature of the recirculating flow within the liquid plugs moving through the microchannel; it has been widely reported that droplet breakup is strongly dependent on immediate shear history, and can be promoted by abrupt changes in the rate of shear, even at subcritical values.[34,35,37] In addition, our simplified treatment of QDCMs as solvent-swollen poly-styrene particles neglects the critical component of the PS-*b*-PAA stabilizing chains (Figure 1), which act as a surfactant by localizing at the polymer/solvent interface. These stabilizing chains will lower the interfacial tension, favoring droplet breakup at lower shear rates; as well, dynamic surfactant gradients over the QDCM/solvent interface in shear flow can influence the critical capillary number and may also promote droplet breakup compared to a clean interface.[34,37,38] Finally, we point out that solvent-swollen QDCMs are viscoelastic and shear-thinning particles, such that non-Newtonian effects will play a significant role in determining their stability and breakup mechanism under high shear.[39,40]

To analyze the liquid flow field within the reactor, a simplified computational fluid dynamics model of the flow within the liquid phase was formulated including the liquid plug and the film surrounding the bubble. Results of the model, formulated in a commercial CFD package (FLUENT 6.2.16), are shown in Figure 5. The model involves several assumptions: the bubble caps are assumed spherical, the liquid film thickness is constant and at 0.1 μm (based on the Bretherton theory[41] and measured surface tension values), the gas phase viscosity is negligible and thus the gas–liquid interface has zero shear, and the channel is circular in cross section, providing a two-dimensional axisymmetric computational domain with a channel diameter related to the microfluidic chip via the hydraulic diameter.[42] Although this simplified axisymmetric model cannot include the full three-dimensional character of this flow (e.g., corner-flow, etc.), the results provide insight into the nature of the flow, the mechanisms and locations of high shear regions, and order-of-magnitude estimates of maximum shear rates in multiphase reactors. The frame of reference translates at the velocity of the liquid plug such that the liquid domain boundaries are fixed relative to the computational domain. Figure 5a shows a schematic of the computational domain with representative superimposed velocity vectors indicating the circulatory motion inside the liquid plug. The expanded view shows shear rate contours in the corner regions where the liquid plug meets the liquid film surrounding the gas phase and where the highest shear rates occur. For a liquid plug velocity of 2.65 mm/s (characteristic of the $Q = 4.8$ μL/min case), the maximum shear rate corresponds to 2×10^4 s^{-1}. Similarly, the maximum shear rate corresponding to the higher flow rate case ($Q = 24$ μL/min) was 1×10^5 s^{-1}. The shear rate

(34) Stone, H. A. *Annu. Rev. Fluid Mech.* **1994**, *26*, 65.
(35) Rallison, J. M. *Annu. Rev. Fluid Mech.* **1984**, *16*, 45.
(36) Bentley, B. J.; Leal, L. G. *J. Fluid Mech.* **1986**, *167*, 241.

(37) Briscoe, B. J.; Lawrence, C. J.; Mietus, W. G. P. *Adv. Colloid Interface Sci.* **1999**, *81*, 1.
(38) Stone, H. A.; Leal, L. G. *J. Fluid Mech.* **1990**, *220*, 161.
(39) Mighri, F.; Haneault, M. A. *Appl. Polym. Sci.* **2006**, *100*, 2582.
(40) Favelukis, M.; Lavrenteva, O. M.; Nir, A. *J. Fluid Mech.* **2006**, *563*, 133.
(41) Bretherton, F. P. *J. Fluid Mech.* **1961**, *10*, 166.
(42) Bird, R. B.; Stewart, W. E.; Lightfoot, E. N. *Transport Phenonmenon*; John Wiley & Sons: New York, 1960.

(a)

(b)
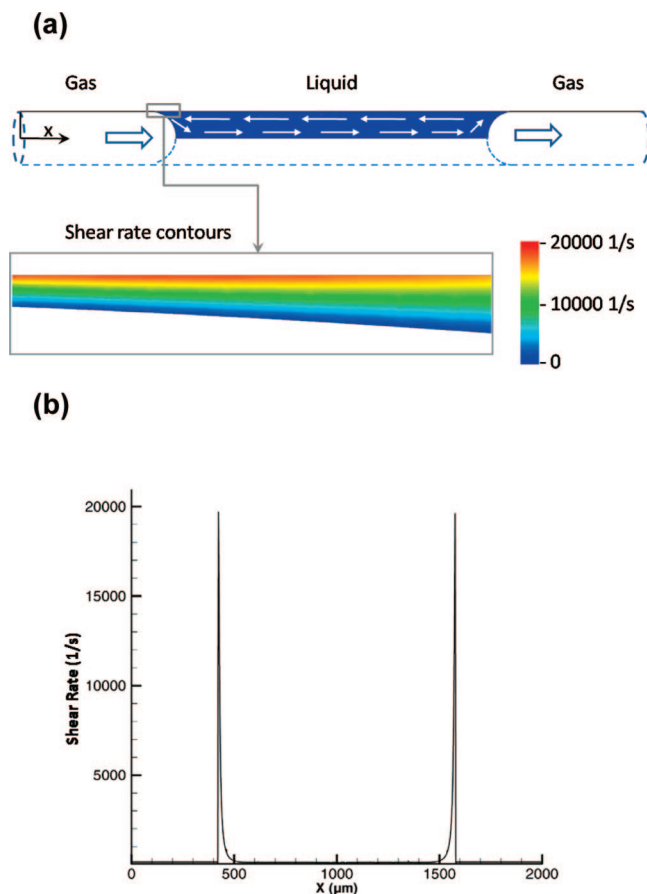
Figure 5. Computational modeling results. (a) Schematic of the computational domain, shown in blue. White arrows indicate the direction of liquid motion within (and relative to) the liquid plug. The model considers axisymmetric flow within the liquid plug between two bubbles in a circular cross section channel. The magnified portion shows shear rate contours corresponding to the $Q = 4.8$ μL/min case in the corner region where the highest shear rates occur. (b) Corresponding axial shear rate profile along the channel wall. The wall shear rate in the central portion of the liquid plug (representative of a single-phase reactor at the same total flow rate) is insignificant as compared to the local shear rates in the corner regions.

at the channel wall for the $Q = 4.8$ μL/min case is plotted versus distance along the plug in Figure 5b. The very large peak values of wall shear rate near the bubble caps are in stark contrast with the rest of the liquid plug, which shows a maximum shear rate (120 s^{-1}) comparable to a single-phase reactor at the same total flow rate. The source of the high shear is the location of the stagnation point (or stagnation line in three dimensions) occurring on the bubble surface very near the imposed velocity at the channel wall. In the reference frame of the laboratory, this high shear rate is a result of the bubble surface imposing a velocity on the liquid near the stationary channel wall.

The calculated ratio of the magnitude of the shear rate to the vorticity indicates a velocity-gradient tensor parameter, α, of approximately 0.1 in the region of high shear within the liquid plugs.[34] In the context of classical droplet breakup results, this value is closer to that of simple shear flow (α = 0) with relatively high vorticity, as opposed to purely elongational, orthogonal flow (α = 1), which would oppose droplet breakup under steady shear conditions.[34−36] However, in the context of the dramatically nonuniform shear conditions present in the liquid plugs, droplet breakup appears to occur even under high-vorticity flow. The

combination of the circulatory nature of the flow field in the liquid plug, and the highly localized regions of high shear stress, should result in a highly unsteady and nonuniform shear exposure for particles circulating within these reactors.

Conclusions

We have applied a two-phase gas-segmented microfluidic reactor to the self-assembly of block copolymers and polymer-coated quantum dots into quantum dot compound micelles (QDCMs). Compared to our previous flow-focusing microfluidic reactor, in which mixing of water with the polymer components was diffusion-controlled, the time of mixing is greatly reduced by chaotic advection within the sinusoidal mixing channel. We find that this enhanced mixing alone is not sufficient to improve QDCM polydispersities compared to our previous results; comparison of the present low shear exposure experiment with an earlier flow-focusing experiment suggests that the mean sizes and polydispersities of the assemblies immediately following self-assembly are largely governed by the steady-state water content, regardless of very different mixing times. However, mean QDCM sizes and polydispersities are both significantly decreased in the post-formation channel by tunable processing of the assemblies, which we attribute to shear-induced particle breakup within the recirculating flow fields of the liquid plugs. We demonstrate that the application of post-formation processing allows the kinetically controlled QDCM sizes and polydispersities to be tuned via the flow rate, which controls the maximum shear rate within the liquid plugs, and via the channel length, which controls the processing time before quenching at a given flow rate. Simple numerical analysis of flow fields and maximum shear rates within the gas-segmented reactor is used to support the feasibility of shear-induced particle breakup, although more detailed theoretical analysis combining the assemblies with the liquid medium is of interest. Although two-phase microfluidic reactors have been previously applied to the fast and efficient mixing of reagents for various chemical processes,[14,27,28] we believe that this is the first example of post-formation processing of nanoscale objects via shear within a microfluidic reactor. Along with providing a fundamentally new handle on size and polydispersity control for the equilibrium and nonequilibrium self-assembly of quantum dots, block copolymers, and other nanoscale building blocks, these results point to intriguing general strategies for the controlled formation of micro- and nanoemulsions via microfluidics.[43,44]

Supporting Information Available: Details of the calculation of interfacial tension between QDCMs and the solvent medium. This material is available free of charge via the Internet at http://pubs.acs.org.

LA8022985

(43) Stone, H. A.; Stroock, A. D.; Ajdari, A. *Annu. Rev. Fluid Mech.* **2004**, *36*, 381.
(44) Fischer, P.; Erni, P. *Curr. Opin. Colloid Interface Sci.* **2007**, *12*, 196.